Mass Inertia Effect based Vibration Control Systems for Civil Engineering Structure and Infrastructure

Chunwei Zhang and Jinping Ou
Harbin Institute of Technology, Harbin, Dalian University of Technology, Dalian,
P.R.China

1. Introduction

In 1972, J.T.P. Yao introduced the modern control theory into vibration control of civil structures (Yao, 1972), which started the new era of research on structural active control in civil engineering field. During the development of nearly 40 years, Active Mass Driver/Damper (AMD) control, with the better control effect and cheaper control cost, has taken the lead in various active control occasions, becoming the most extensively used and researched control systems in lots of practical applications (Soong, 1990; Housner *etal.*, 1997; Spencer *etal.*, 1997; Ou, 2003). Several important journals in civil engineering field, such as ASCE Journal of Engineering Mechanics (issue *4th*, in 2004), ASCE Journal of Structural Engineering (issue *7th*, in 2003), Earthquake Engineering and Structural Dynamics (issue *11th*, in 2001 and issue *11th*, in 1998), reviewed the-state-of-the-art in research and engineering applications of semi-active control and active control, especially AMD control. In addition, Spencer and Nagarajaiah (2003) systematically overviewed the applications of active control in civil engineering. Up to date, more than 50 high-rising buildings, television towers and about 15 large-scale bridge towers have been equipped with AMD control systems for reducing wind-induced vibration or earthquake-induced vibration of the structures.

Besides, there are quite a number of successful applications with passive Tuned Mass Damper (TMD) control system, from wind induced vibration control of long-span bridge towers and building structures, to chimneys and mast structures; from the first applications of the collapsed World Trade Center towers and coetaneous John Hancock building etc., which were built in 1960s, to recently built highest structures in the world, *e.g.* Twin towers in Kulua- Lumpur in Malaysia, 101 skyscraper in Taipei city and Guangzhou New TV tower in China etc. It can be seen from these applications, the implementation of incorporating Mass Driver/Damper based vibration control systems for protection of Civil Engineering structures and infrastructures against wind and earthquake excitations, have already been widely accepted by the field researchers as well as engineer societies.

2. EMD control systems

Zhang (2005) made a systematically comparison for different control schemes under the background of the Benchmark control problem, and disclosed that the AMD control was the

best control scheme due to these merits, such as the best ratio of control effect over control effort, simple and easy to be implemented etc. Moreover, through analysis of typical important large-scale structures subjected to different excitations, the effectiveness and feasibility of employing AMD control for civil structures has been successfully proven (Ou, 2003; Zhang, 2005), where wind and earthquake induced vibration control of high-rising buildings and bridge towers, ice induced vibration control of offshore platforms, wind-wave-current coupling excited control of deep sea platforms are all studied. Usually, an AMD control system is composed of a mass piece, an actuator, stiffness component (coil spring is commonly used), a damper, a stroke limiting device, a brake protector, sensors, a data acquisition and processing system, computerized real-time control software and hardware system (Dyke *etal.*, 1994, 1996; Quast *etal.*, 1995; Spencer *etal.*, 1997). In addition, a power supplying system is needed for operating all the electrical devices mentioned above.

In traditional AMD system, the mostly used actuators are hydraulic cylinders or electrical servo motors, which may have the following disadvantages, such as large in system volume, complicated in construction, time delay, slow to response, and limited mass stroke etc. Aiming at this, several new special devices were put forward to replace the traditional actuators (Haertling, 1994, 1997; Nerves, 1996; Scruggs, 2003). Learning from the motion control principle of magnetic suspended vehicle, the electromagnetic mass damper (subsequently called the "EMD") control system, as an innovative active control system, was proposed for structural vibration control (Zhang, 2005), which uses the driving technology of linear electric machines, transforming the electric energy directly into mechanical energy of EMD system, for example, the kinetic energy of EMD mass. Figure 1(a) shows the conception sketch of hydraulic actuated AMD system and its implementation illustration in a typical structural model, as shown in figure 1(b). By comparison, figure 2(a) and 2(b) shows the corresponding sketch and implementation sketch of the EMD control system.
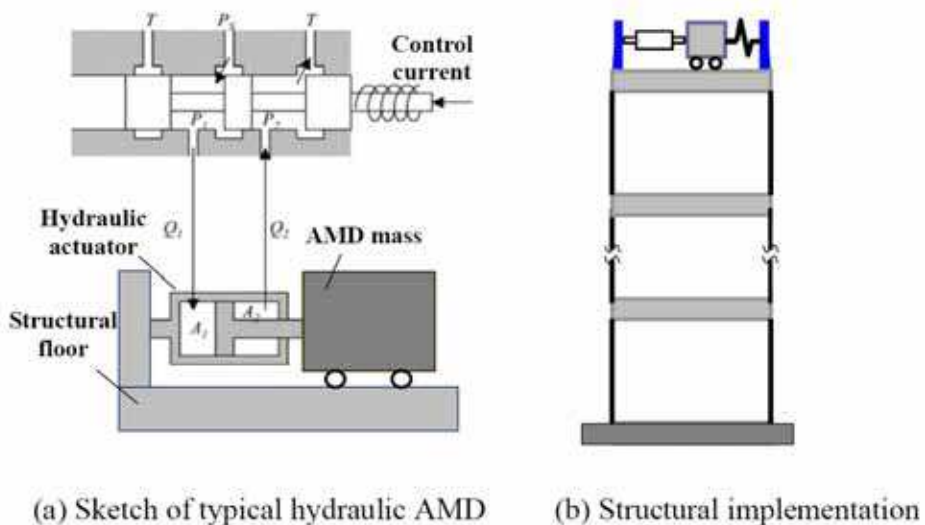

(a) Sketch of typical hydraulic AMD   (b) Structural implementation

Fig. 1. Sketch of structure with hydraylic actuated AMD control System

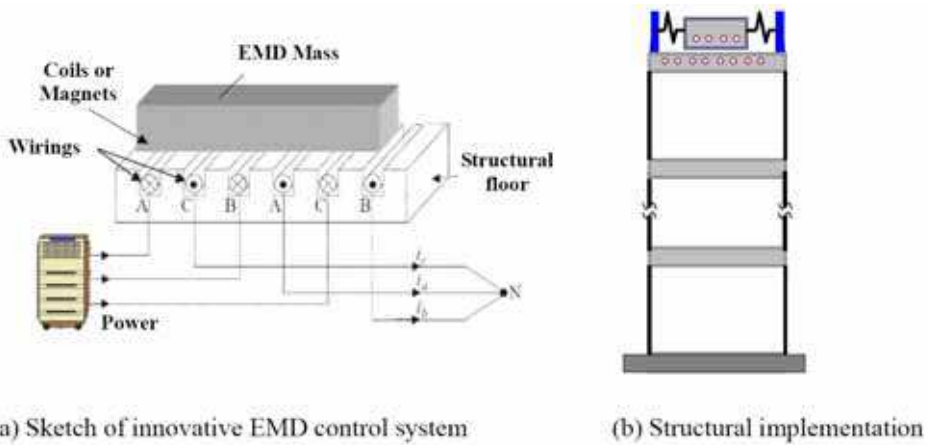(a) Sketch of innovative EMD control system   (b) Structural implementation

Fig. 2. Sketch of structure with Electromagnetic Mass Damper (EMD) contol system

2.1 Miniature EMD control system

The miniature experimental EMD control system is composed of a mass piece (direct current excitation coils encapsulated in high-strength engineering plastics, with mounting holes on its surface), a permanent magnet rod made of high energy rare earth material, linear sliding bearings and the system chassis. In addition, in order to form a closed-loop EMD system, an optical scale and an accelerometer are integrated into the EMD system to measure the stroke and absolute acceleration of the mass, respectively. Photo of the whole integrated system is shown in figure 3.
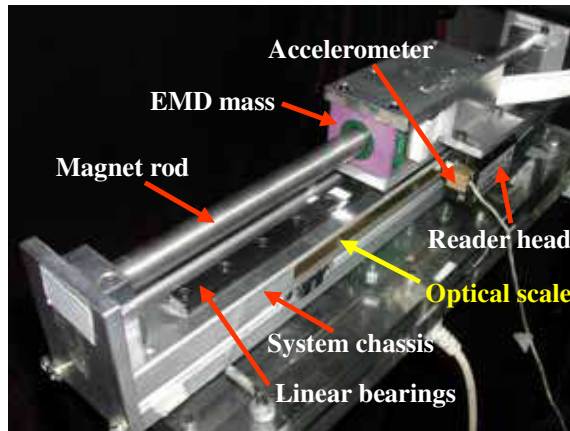

Fig. 3. Integrated photo of the EMD actuator

The excitation coil in the sealed mass package is 87mm long, made by Copley Controls Inc., and the whole mass piece weighs 186 grams. The permanent magnet rod is 332mm long with the diameter of 11mm. The main electrical specifications of this EMD system are: peak force constant is 5.74N/A, root mean square (RMS) force constant is 8.12N/A, back electro-

motive force (EMF) constant is 6.63 V·s/m, the coil resistance at 25°C is 5.35 Ω, and the coil inductance is 1.73mH. The mass stroke of EMD system is measured using a Renishaw optical scale, which is pasted onto the system chassis as shown in the photo above, while the reading head is fixed on the side wall of EMD mass. The reading head model is RGH24 with the resolution of 2-micro-meter, and the scale is 220mm long. In addition, one tiny accelerometer (type DH201-050) is installed on the prolonging side-wall of the EMD mass with the measuring range of ±50g. This accelerometer is very compact indeed, with a weight of only two grams and a volume of 10mm×10mm×5mm, and it can be conveniently attached to any part of the mass piece without influencing the operation of the whole system.

2.1.1 System mathematical models

From the aspect of circuit calculation, the armature of EMD system consists of three parts: motor coil which is capable of outputting mechanical force or energy, coil inductance and coil resistance. According to the Kirchhoff's first principle, the relationship of the circuit voltage and current can be written as

$$L_m \frac{di(t)}{dt} + R_m i(t) + \varepsilon(t) = V_m(t) \tag{1}$$

Where L_m is the coil inductance, R_m is the coil resistance, $V_m(t)$ is the input voltage, $\varepsilon(t)$ is the inducted back EMF constant, $i(t)$ is the current intensity in the coil.

Defining the following two electric indices of linear motors, $K_f = \dfrac{F_{\text{EMD}}}{I}$ standing for force constant which means electromagnetic force generated by unit current input, and $K_m = \dfrac{\varepsilon}{v}$ standing for the back EMF constant which means back EMF generated by unit velocity, then the following relationships are reached,

$$i(t) = F_{\text{EMD}} / K_f \; ; \; \varepsilon(t) = K_m v \tag{2}$$

Substituting equation (2) into equation (1) gives

$$L_m \frac{dF(t)}{dt} \frac{1}{K_f} + \frac{R_m}{K_f} F(t) + K_m v(t) = V_m(t) \tag{3}$$

After proper transformation, equation (3) can be rewritten as,

$$F(t) = \frac{K_f}{R_m} V_m(t) - \frac{K_f K_m}{R_m} \dot{x}_a(t) - \frac{L_m}{R_m} \frac{dF(t)}{dt} \tag{4}$$

Where $\dot{x}_a$ is the relative velocity of EMD mass, and $F(t)$ is the controllable electromagnetic force.

2.1.2 System dynamic tests

During dynamical tests, the EMD system is fixed on the shaking table, and the system coil is powered with the ASP-055-18 servo amplifier, with a DC current output of 0~10A and voltage of 0~55V. The power supply is the HB17600SL series regulator module. A series of

sine position based tests under Position-velocity control of large mass strokes and low frequencies are conducted.

For example, figure 4 shows the hysteresis loops of control force versus velocity and circuit current, respectively. From the force-current relationship, fine linear relationship again indicates the EMD system to be a linear actuator under low operating frequencies, with high ability in dissipating energy at the same time.
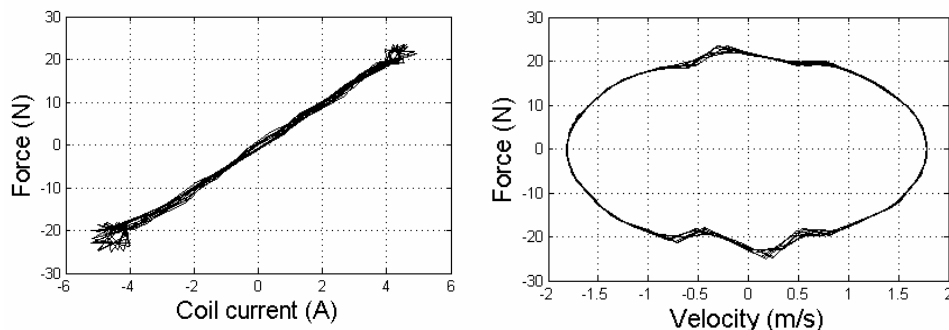

Fig. 4. Force hysteresis loops of EMD system

2.1.3 Experimental implementation of structural model

The test structural model employed in this part is a two-story shearing type structure, called the Bench-scale structure, manufactured by Quanser Inc., which has been designed to study critical aspects of structural control implementations and widely used in education or research of civil engineering and earthquake engineering throughout the world (Battaini, 2000; Quanser, 2002). The column of the test structure is made of thin steel plate, 2mm thick, and the floors are made of plastic, 13mm thick, and the inter-storey height of the structure is 490mm. Shaker-II table, made by Quanser Inc., is employed here for generating earthquake excitations as well as other excitations to be exerted onto the test structure. Through sine sweep test, the natural frequencies of the structure are found to be 1.27Hz and 4.625Hz corresponding to the first two dominant vibration modes respectively, where the mass of the EMD system is fixed on the top floor, named as uncontrolled case. The photo of the whole experimental system and its calculation sketch are shown in figure 5.

In the current experimental setup, two accelerometers are installed under each floor and another accelerometer ia installed on the shaking table surface to measure structural response and input excitation respectively. The acceleration transducers are the type of Kistler K-Beam 8034A with the measuring range being ±2.0g and the sensitivity gain being 1024mV/g. Two laser displacement sensors, type of Keyence LK-2501/2503, are employed to measure the absolute displacement of each floor of the structure, which both work under the long distance mode, and the measuring range is ±250mm with the gain being 200mV/cm. Here the displacement measurement is used only for verification purpose, while not for feedback.

In this section, shaking table tests of structural seismic response control employing the EMD system were conducted, where three benchmark earthquake waves were used as input to examine the control effectiveness of such an innovative active control system, and typical results under Kobe earthquake wave (NS, January 17, 1995) input will be shown in the
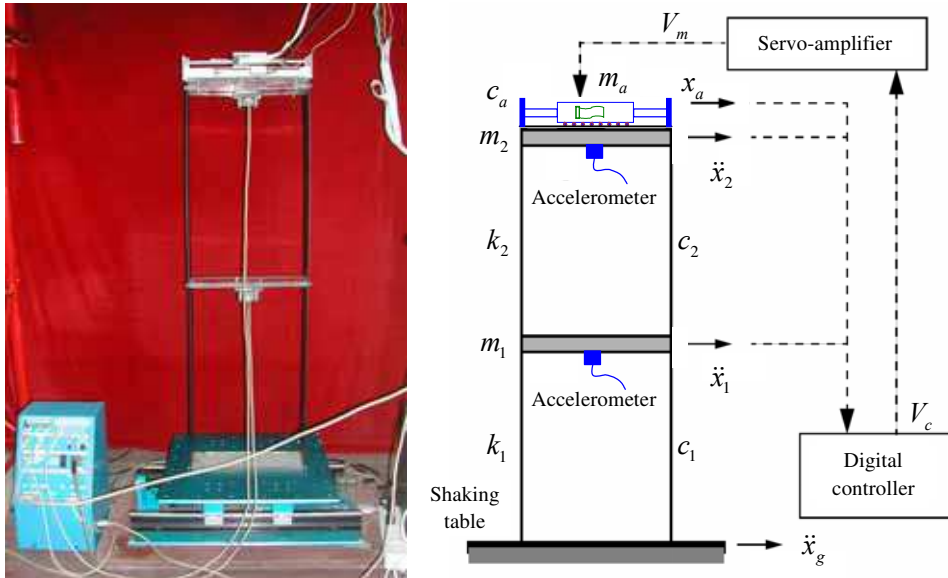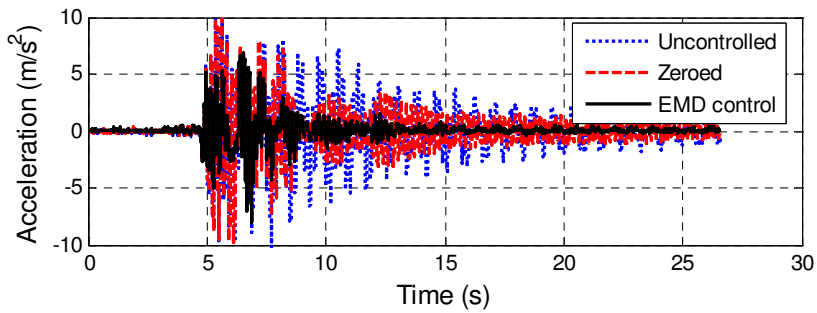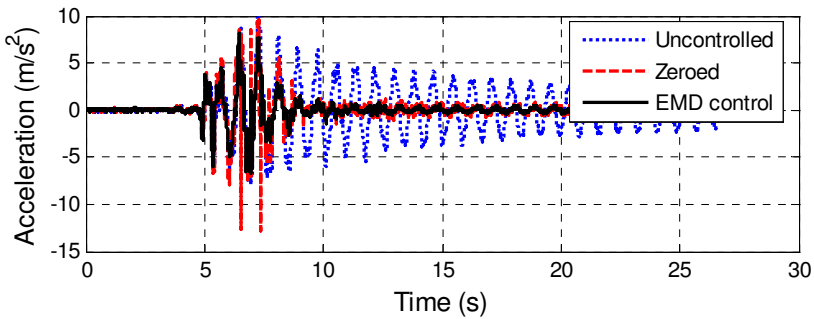
Fig. 5. Photo and calculation sketch of whole system
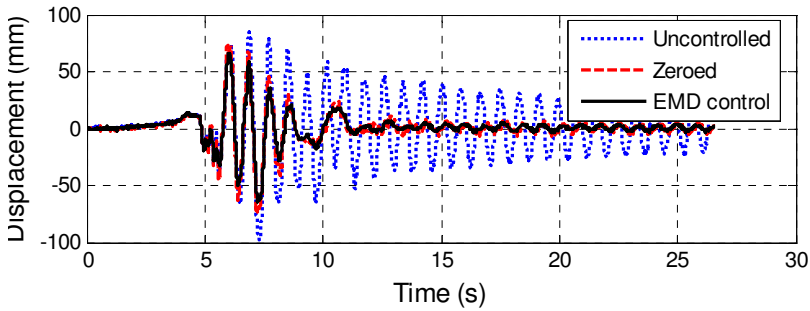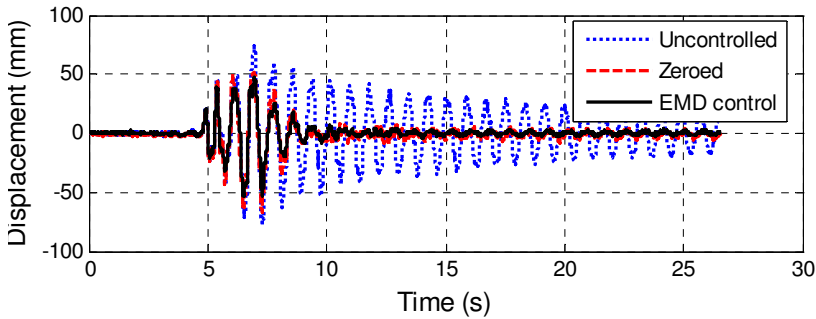

(a) Absolute acceleration of the first floor

(b) Absolute acceleration of the top floor

Fig. 6. Experimental structural acceleration under Kobe wave excitation

(a) Absolute displacement of the first floor

(b) Inter-drift of the top floor

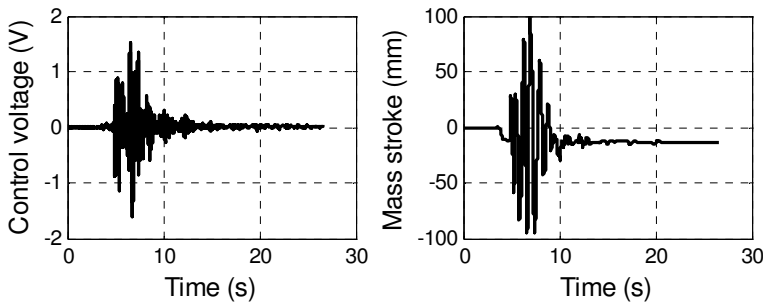Fig. 7. Experimental structural displacement under Kobe wave excitation

Fig. 8. Time history of control voltage and mass stroke of EMD system under Kobe wave excitation

following part. During the experiment, laser transducers are used to measure the absolute displacements of each floor of the test structure, and the inter-storey deformation can be calculated through subtraction of displacements of adjacent floors.

Figure 6 and figure 7 show the comparison of the structural absolute acceleration and floor displacement and inter-drift under three cases, Uncontrolled, Zeroed and EMD active control respectively. From the results, the EMD control is shown to be the most effective in suppressing structural vibrations. In addition, time histories of control voltage and mass stroke of the EMD system are also shown in figure 8.

In the above, theoretical modeling, dynamical testing, shaking table tests have been systematically carried out for the miniature EMD control to investigate its feasibility for using in structural vibration control. All the results show it to be a promising active control system for civil engineering.

2.2 Benchmark scale EMD control system

The existing linear motor products are already getting so close to rotatory motors in velocitty regulation area, and the products are mostly low power motors to drive the AMD mass (Zong etal.,2002). Requested performances of AMD system used for vibration control of civil engineering structures are high power, heavy load and high response ability to frequency, however control accuracy is not necessarily requested. Sometimes the servo motor power may exceed hundreds or thousands of Kilowatts. One of the possible means to solve the problems is to use simple tri-phase asynchronous linear motors in the design of full scale AMD control system.

An approach of setting up the high power linear electrical motor servo system is studied in this part. To build the high power position servo system, normal frequency transducer is used to drive an asynchronous linear motor. Because the mathematical model of asynchronous motor is not easy to set up, a new controller design method based on the step response of the closed-loop system is introduced, and series of numerical simulations and experimental verifications were carried out. Experimental results showed that good control performance can be achieved using the designed controller for the physical system.

2.2.1 Principles of position control for asynchronous linear motor

Constitution of traditional rotatory position servo systems is shown in figure 9. In the traditional structure, rotatory machines and ball bearing screw are used, and the mass load is driven to perform linear motion. Due to the avoidless clearance between screw and load, transmission accuracy gets declined and the servo rigidity is affected. Linear motors are taken in to drive the load in the linear electric motor position servo system shown in figure 10. Without transmission components and movement transform, higher transmission accuracy and servo rigidity are achieved from asynchronous motors. At the same time, higher accuracy and dependability are achieved from whole position closed-loop system with raster ruler instead of rotatory encoder than half closed-loop system.
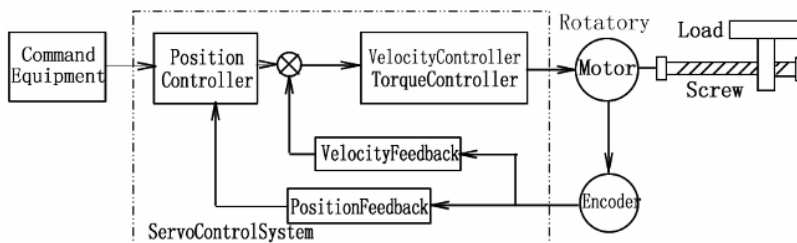

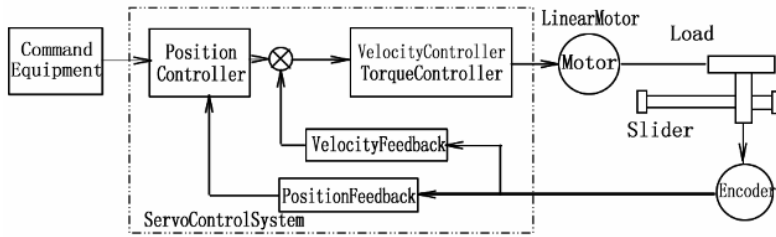Fig. 9. Sketch of Rotary Servo System for Position Control

Fig. 10. Sketch of Linear Servo System for Position Control

Applications of linear motors focus on low power situations such as disk reader, printer, and numerical machine tools, so high power linear motion servo driver equipments can't be purchased. All the correlative hardware equipments have to be designed independently (Ye, 2003). This part takes vector alternating frequency transducer driver and asynchronous linear motor instead of position servo system, and makes use of computer servo control card to perform the controller's function, then builds the integrated servo system with asynchronous linear motor. The frame of the whole system is shown in figure 11.

From figure 11, functions of the components are shown: Control computer plays the role of servo controller. The position command signal is generated in MatLab/Simulink. Position error is calculated out from position command and position feedback from raster ruler, then velocity command signal is calculated, at last velocity voltage is produced from real-time control software WinCon and servo control card to frequency transducer. The linear motor is driven by the frequency transducer to run at the assigned speed according to the velocity command. The load is driven by the linear motor to perform linear motion displacement following the position command.
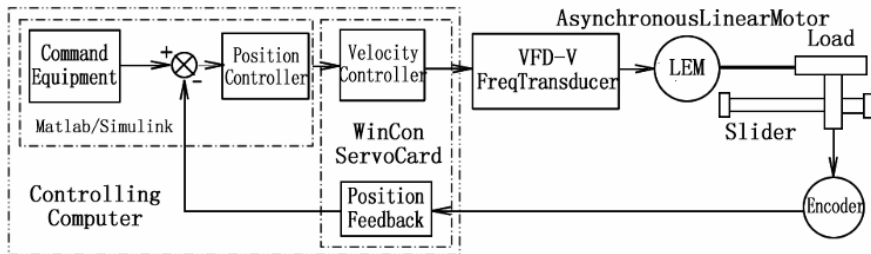

Fig. 11. Position Control of Asynchronous Linear Motor

Based on the structure shown in figure 11, equipments are chosen according to the power requirement. A tri-phase asynchronous linear motor with the power 4.5 kW, synchronous speed 4.5 m/s (50 Hz) is ordered, and a speed slip of 0.05 (5%) is estimated from experiments. The linear motor driver is Delta VFD-V model, high performance vector tri-phase alternating frequency transducer, with driving power of 5.5 kW. Position feedback tache is the most important component of the whole system, so a raster ruler produced by Renishaw Co. is chosen. Model of the ruler reader is RGS20, and minimal resolving power of the raster is 20 um. MultiQ-3 servo control card produced by Quanser Co. is setup in the control computer, with software of WinCon3.2 and Matlab 6.0. Structure of the whole

asynchronous linear electric motor is shown in figure 12. Figure 13 shows the picture of the experiment equipment and the software runtime is shown in figure 14.
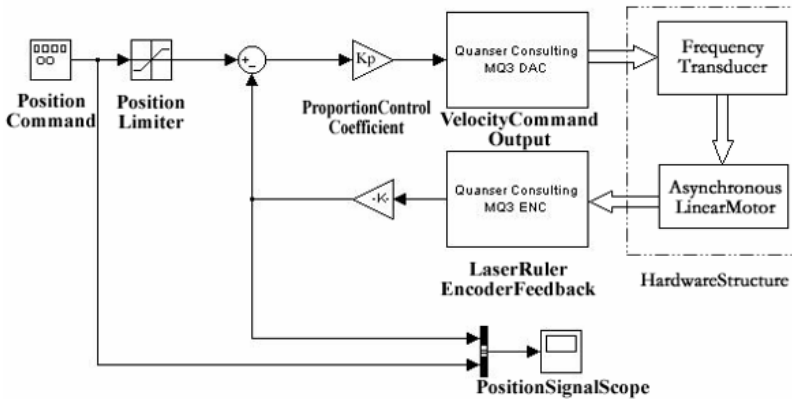

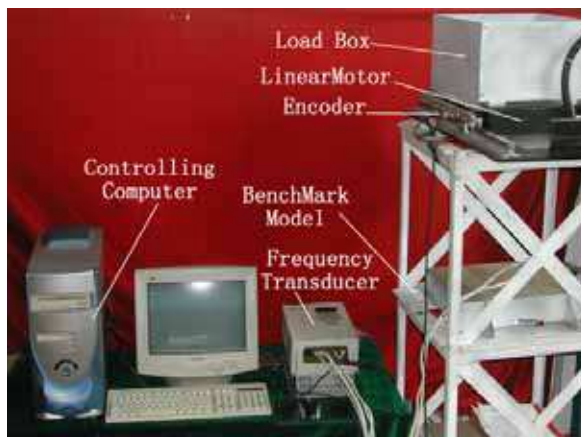Fig. 12. Structure of the Position Control System

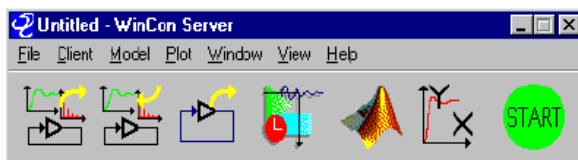Fig. 13. Picture of the Control System

Fig. 14. Picture of the running WinCon

2.2.2 System model and position controller design

Traditional control method and controller design is commonly based on mathematics model of the object under control, and the controller is calculated according to required performance. Generally, mathematics model of the system is obtained by the method of analyze or system

identify, estimating model from the input and output experimental data. For the mathematic expression of asynchronous linear motor is so complex and parameters the manufacturer offered is not enough to build the model from analyze. At the same time, experiment situation of linear motor is limited by dimensions of the platform, so experiments can't be implemented to get enough data system identify required, which makes design of the controller much more difficult. In the engineering problem design process, simplification of the mathematics model usually makes the controller difficult to actualize or get awful performance. So a simple and facile approach that fits the engineering application is necessary.

This part analyzes and summarizes most of the design methods and tries a new design method. Reference to the design method of Extraction of Features of Object's Response, briefly EFOR, an approach to design the Lag-Lead compensator based on the experimental step response of the closed-loop system is implemented and good performances is achieved. Basic idea of quondam EFOR method is described as below: closed-loop simulation is carried out to a series of "Normal Object", to get the step response, and then some main time characteristic parameters are read out, and the controller is designed according to the parameters. The "Normal Object" is provided with some special characters: transfer function is strict proper rational point expression or proper rational point expression; minimum phase; at most one layer integral calculus; magnitude-frequency character is monotonous reduced function to the frequency (Wu etal., 2003).

Experiments showed that the asynchronous linear motor system couldn't satisfy all the requirement of the "Normal Object", especially the magnitude-frequency character is not monotonous reduced function to the frequency. But the step response of closed-loop system is similar to the attenuation oscillatory of the second-order system, so the EFOR method could be attempted to design the controller. So reference to the EFOR design method, a new method of Lag-Lead compensator design based on the experimental test is tried to accomplish the controller design. Detailed design process is shown below:

a. Step response experiment is carried out, especially the curve of high oscillatory with similar amplitudes, and attenuation oscillatory periods T_d is obtained, and then the frequency of system attenuation oscillatory $\omega_d = 2\pi / T_d$ is calculated, at last the critical attenuation oscillatory ω_p is estimated; The experimental method is especially fit for some systems which only perform movement within limited displacement such as linear electric motors. These systems have only limit experiment situation and can't perform long time experiments. The curve of high oscillatory with similar amplitudes when the proportion control coefficient is Kp=15 from the experiments is shown in figure 15. Parameters below are obtained:

$$T_d = 2.926 - 1.702 = 1.224s \tag{5}$$

$$\omega_p \approx \omega_d = 2\pi / T_d = 5.133 rad / s \tag{6}$$

The Lag-Lead compensator is designed according to equivalence oscillatory frequency. Structure of the lead compensator is shown below:

$$K_h(s) = \frac{\dfrac{s}{\omega_m / \lambda} + 1}{\dfrac{s}{\lambda\omega_m} + 1} = \lambda^2 \frac{s + \dfrac{\omega_m}{\lambda}}{s + \lambda\omega_m} \qquad (\lambda > 1) \tag{7}$$

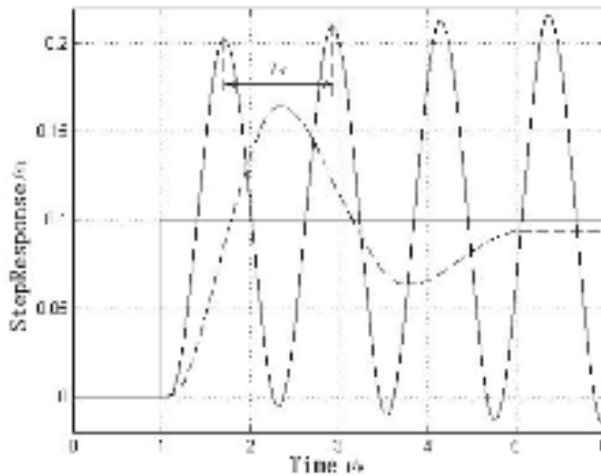Design of the lead compensator is mainly the chosen of parameters λ and ω_m .

Fig. 15. Curve of Critical Oscillating System from Experiments

Parameter λ is named compensator strength. Larger λ produces plus phase excursion and better performance; too larger λ produces phase excursion increased not evidently, but makes the higher frequency gain so large that the high frequency noise is enlarged. So the λ should be selected based on the exceed quantity λ, usually from the empirical formula

$$\lambda = \{ \begin{array}{ll} 1.2 + 4\sigma & (\sigma \le 0.6) \\ 3.6 & (\sigma > 0.6) \end{array} \tag{8}$$

So the compensator strength for the current system is $\lambda = 3.6$.

The compensator mid-frequency ω_m should be a little higher than ω_p . For the second-order system, usually from the empirical formula $\omega_m = \sqrt{\lambda}\omega_p$, so

$$\begin{aligned} \omega_m = \sqrt{\lambda}\omega_p = \sqrt{3.6} \times 5.133 \\ = 9.740 rad/s \end{aligned} \tag{9}$$

Thereby the lead compensator is achieved:

$$K_h(s) = \frac{\dfrac{s}{\omega_m/\lambda}+1}{\dfrac{s}{\lambda\omega_m}+1} = \frac{0.37s+1}{0.0285s+1} \tag{10}$$

b. The main purpose of the lag compensator is to reduce the stable error, but phase will usually be reduced, too, so the lag compensator parameters should be determined by the steady error after the lead compensator added. For the system that the error fits the requirement, a lag compensator is not necessary. Usually structure of the lag compensator is like this:

$$K_1(s) = \frac{s+\omega_1}{s+\rho\omega_1} \tag{11}$$

In the expression, the compensator strength is $0 < \rho < 1$. ω_1 is the seamed frequency of the lag compensator, so it must be lower than magnitude crossing frequency ω_c and not close to ω_c, to reduce the effect to mid-frequency performance. Usually $\omega_1 \approx (0.1 \sim 0.2)\omega_c$, $\rho = 1 / n$, so that the steady error could be reduced to $1/n$。

Accordingly, the position controller is designed for the system. The perfect proportion control coefficient is Kp=8. Figure 16 shows the controller structure.

Fig. 16. Structure of Lag-Lead Controller

2.2.3 Simulation and experimental results

The lag-lead compensator based on the step response is $K_h(s) = (0.37s + 1) / (0.0285s + 1)$, and the perfect proportion control coefficient is Kp=8. With the method of getting controller coefficient from test-run, the best perfect coefficient for only proportion controller is Kp=8, and the best perfect coefficient for proportion differential controller is Kp=8, Kd=0.4. The coefficients are applied in the simulations and the experiments below.

By analyzing parameters of the lag-lead compensator and some conclusion from system identification, a simplification model was estimated to test the performance of the controllers. Simulations using different controllers such as lag-lead compensator, proportion controller, or proportion differential controller were carried out with the help of Matlab software. Simulation result with different controllers is shown in figure 17.
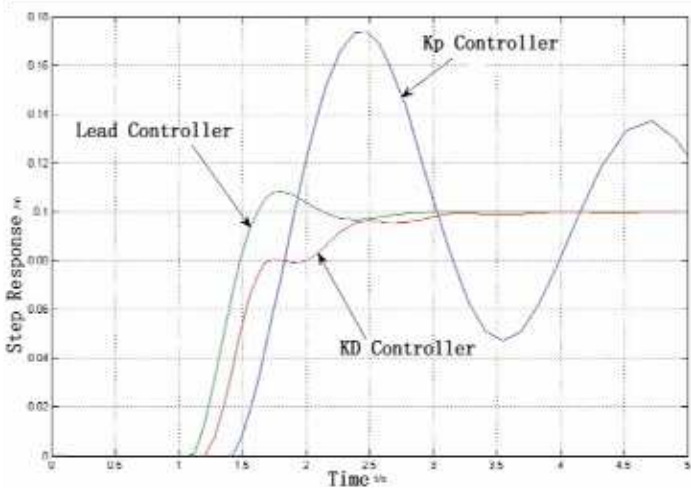

Fig. 17. Results of the Simulations using three different controllers

The figure shows that the lead compensator and the proportion differential controller make great improvement to the object under control. Compared with simple proportion controller, the response speed and the position control error are reduced a lot.

Some experiments were performed on the mechanic equipments. Figure 18 shows the performance of the lead compensator while adjusting the proportion coefficient near *Kp*=8. The performance of following ability test under the lead compensator is shown in figure 19. Obvious following effect to the sine position command with magnitude 50mm and frequency 1Hz is obtained.
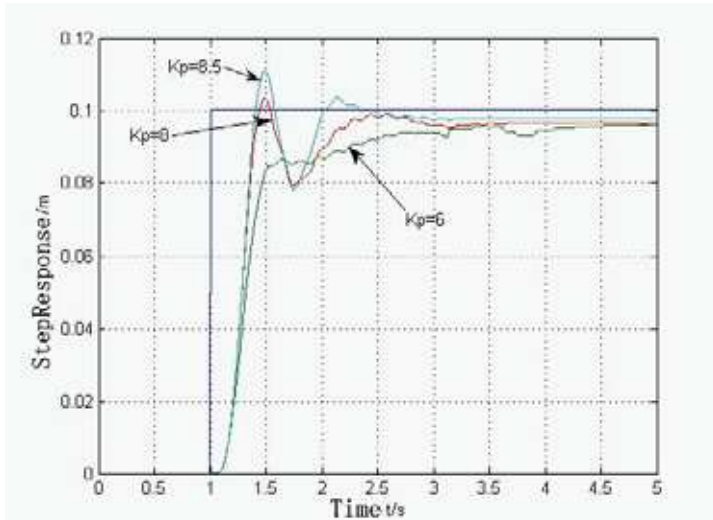

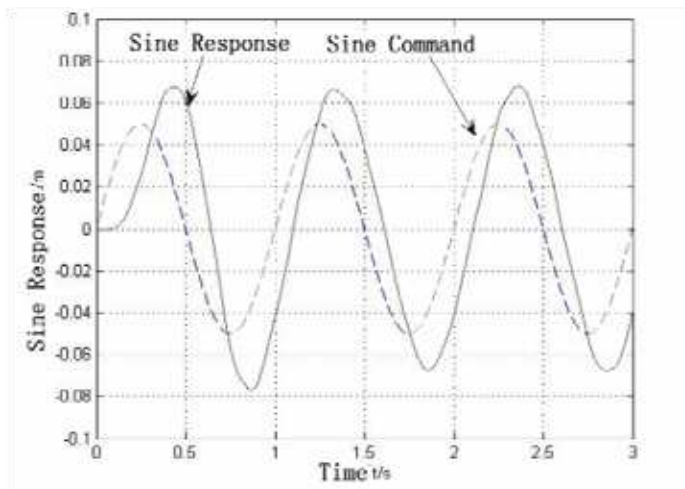Fig. 18. Experiment Results using different Kp

Fig. 19. Experiments Curve of Sine Signal Response

Based on the experiments, the performances of the three different controllers are shown in figure 20.
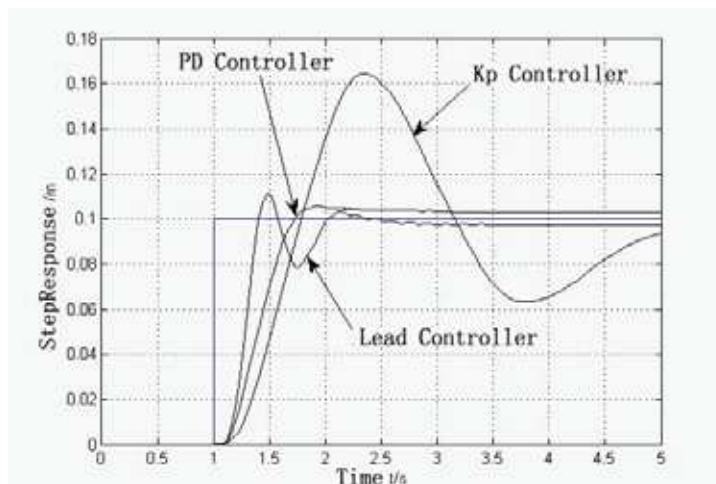
Fig. 20. Comparison of the Experiment results using three different controllers

The following function parameters based on step response are obtained from figure 20.

System Function Value	ising Time/s	ransit Time/s	Surpass Amounts	teady Error	Oscillation Number
LagLeadcontroller	.37	.96	11.5%	%	2
KD Controller	.62	.97	6%	%	1
Kp Controller	.73	.9	64%	%	3

Table 1. Comparison of Function Values from Experiments using three different controllers

The functional parameters shows that the controller designed by the method based on the experimental step response of the closed-loop system improves the system performance a lot, even much better than the proportion differential controller, while the design process is far simple than the design of PD controller.

2.3 Energy harvest EHMD control system

In the following figure 21, the main parts of the innovative EHMD system and their relations were illustrated, respectively. The EHMD system can be divided into the following parts: TMD subsystem with energy dissipating and recycling functions, power module which can preserve and release electrical energy, EMD subsystem which is directly driven by electro-magnetic force. To be specific, TMD damper is replaced by coils embedded fly-wheels combined with high-power batteries, EMD active force is realized using soft magnetic material actuator and high-power capacitor; besides, the standard DSP module is incorporated to make up a real-time control system. The fly-wheels is composed of wheel body, reducer or accelerator using gear boxes, energy generating and dissipating coils, high power storage battery and capacitor, electronic and electrical regulator, as well as mechanical couplings and attachments etc. Considering the fly-wheel battery is relatively a matured technique, here the EHMD should be focused on solving its control strategies to realize a reasonable energy preserving-releasing process for structural active control.
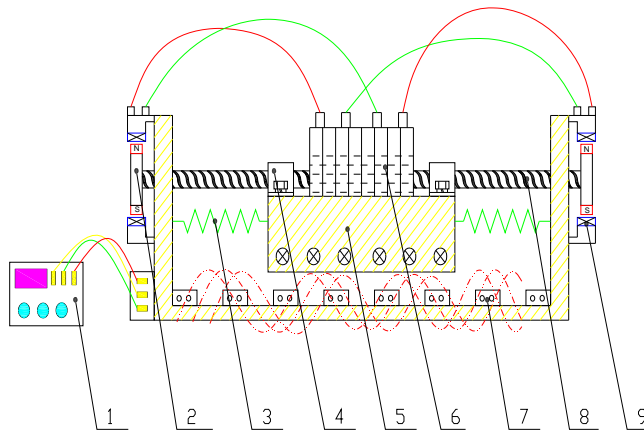
(Note: 1-digital controller, 2-fly-wheel(s), 3-spring element, 4-mechanical couplings, 5-system mass (embedded coils), 6-energy-storing battery, 7-excitation coils, 8-bearings and system rails, 9-permanent magnets)

Fig. 21. Structural integration photos of EHMD system

In the following figure 22, analysis and design procedure of the EHMD system is proposed. First, aiming at the requirement of the specific structure to be controlled, optimal mass ratio, stiffness and damping coefficients, maximum mass stroke and peak control force were calculated, which were set as the hardware standard parameters of the moderate scale EHMD system. Second, applying relevant research results, such as linear motor technique in magneto suspension trains and energy accumulation technologies in fly-wheel batteries etc, key parts of energy recycling, preserving and utilizing for driving EHMD system would be developed. At last, integrating DSP based data acquisition, processing and real-time control modules, the whole experimental EHMD system are fabricated and integrated.

When the structure vibrates, the mass moves driving the couplings rotating which transforms linear motion into rotation, and the embedded coil cut the magnetic field and generates induction currents and stored in the batteries which will be utilized at a
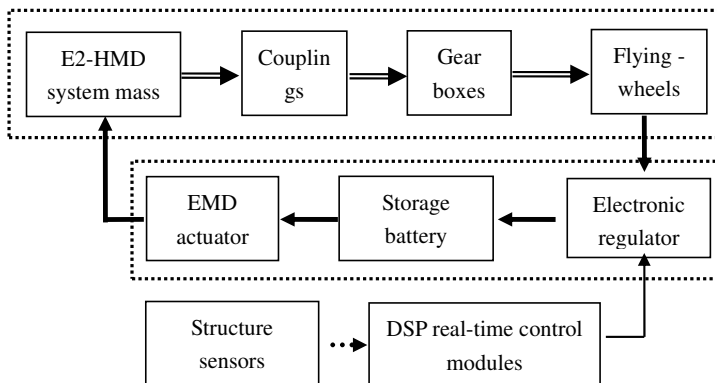

Fig. 22. Structural construction sketch of EHMD system

reasonable occasion. If reducer or accelerator is incorporated into the system, then the efficiency of generating electrical power can be greatly improved, through calculations the optimal gear ratio and damping coefficient can be achieved.

In the following, feasibility of utilizing such kind of EHMD system for suppressing structural vibrations will be considered. Basically, the main problems will be focused on the electrical loops of the system, because the other two major parts will be benefited from AMD and TMD control techniques. Currently, a high-power capacitor can be stored with energy of up to 3MJ, where its energy density will be 1.35kJ / kg and about 1.5kJ / dm^3, thus the mass will be about $2m^3$ and the weight will be 2tons or so, which can power the EMD actuator in continuous working mode for more than 200 seconds. From the data, the EHMD for protection of structural seismic response is absolutely feasible.

3. DDVC based AMD control system

This DDVC based active mass driver control system is proposed for low frequency vibration and motion control, *e.g.* wave induced motion control of offshore platform structures. DDVC (Direct Drive Volume Control) technology comes from the hydraulic industry, which utilizes integrated pump and motor to replace servo valve from traditional hydro cylinders, and to realize such functions as pressure control, speed control and changing working directions etc. DDVC control is also called as valve-less control, which uses servo AC motors driving fixed displacement pumps. DDVC is operated based on regulating rotary speed of pumps rather than changing its flow, and to control actuating speed of actuators. DDVC has been widely researched by institutions from Japan, USA, German, Sweden and China. The most common applications are used in such industries as high-precision forging machinery, ship helms, heavy load casting machineries, printing machines, 6-DOF platforms and rotary tables, 2500 ton inner high pressure shaping machine, operating switch for floodgates etc. Besides, some applications have been proposed for aerospace engineering (also called EHA, Electrical Hydro Actuator) recently because the most attracting advantages of compact volumes, high energy saving efficiencies etc.

Figure 23 shows the photo of one typical DDVC system fabricated by 1st Japan Electric Corporation. DDVC-AMD is an innovative replacement of actuator from traditional hydro cylindrical AMD control system, and figure 24 shows the working principles of such DDVC actuated AMD control system.

Fig. 23. Photo of DDVC driver

Thank You for previewing this eBook

You can read the full version of this eBook in different formats:

  ➢ HTML (Free /Available to everyone)

  ➢ PDF / TXT (Available to V.I.P. members. Free Standard members can access up to 5 PDF/TXT eBooks per month each month)

  ➢ Epub & Mobipocket (Exclusive to V.I.P. members)

To download this full book, simply select the format you desire below